arXiv:1209.4229v1 [cond-mat.supr-con] 19 Sep 2012

Nodeless superconductivity in $Ir_{1-x}Pt_xTe_2$ with strong spin-orbital coupling

S. Y. Zhou,[1] B. Y. Pan,[1] X. Qiu,[1] J. Pan,[1] X. C. Hong,[1] X. L. Li,[1] Z. Zhang,[1]
J. J. Yang,[2] Y. S. Oh,[3] S-W. Cheong,[2,3] and S. Y. Li[1,*]
[1]*State Key Laboratory of Surface Physics, Department of Physics,*
and Laboratory of Advanced Materials, Fudan University, Shanghai 200433, P. R. China
[2]*Laboratory for Pohang Emergent Materials and Department of physics,*
Pohang University of Science and Technology, Pohang 790-784, Korea
[3]*Rutgers Center for Emergent Materials and Department of physics & Astronomy,*
Rutgers University, Piscataway, New Jersey 08854, USA
(Dated: September 20, 2012)

The in-plane thermal conductivity κ of the layered superconductor $Ir_{1-x}Pt_xTe_2$ singe crystal was measured down to 50 mK. In zero field, a finite residual linear term κ_0/T is observed, which is usually considered as the signature of nodal superconducting gap. However, in magnetic field, κ_0/T decreases first, then increases slowly with increasing field. This field dependence of κ_0/T is inconsistent with nodal gap. We attribute the finite κ_0/T in zero field and the decrease of κ_0/T in low field to the nonsuperconducting impure phase in the crystal. The overall slow field dependence of κ_0/T manifests the underlying nodeless superconducting gap in $Ir_{1-x}Pt_xTe_2$, which puts strict constrain on the pairing symmetry.

PACS numbers: 74.25.fc, 74.40.Kb, 74.25.Op

The effect of strong spin-orbital coupling (SOC) on superconductivity has recently attracted much attentions. One example is the topological superconductor, such as candidate $Cu_xBi_2Se_3$ in which Cu atoms are intercalated into topological insulator Bi_2Se_3 with strong SOC.[1] Novel superconducting state was claimed in $Cu_xBi_2Se_3$ by the point-contact spectra and superfluid density measurements.[2,3] Another example is the noncentrosymmetric superconductor, such as Li_2Pt_3B in which the spatial inversion symmetry is broken.[4] The strong SOC in Li_2Pt_3B gives large spin-triplet pairing component and produces line nodes in the superconducting gap.[5,6]

Very recently, superconductivity was discovered in the layered compound $IrTe_2$ by Pd intercalation (Pd_xIrTe_2), Pd substitution ($Ir_{1-x}Pd_xTe_2$), or Pt substitution ($Ir_{1-x}Pt_xTe_2$).[7,8] The parent compound $IrTe_2$ shows a charge-orbital density wave (DW) type transition at $\sim$ 262 K.[7] With increasing the doping level x, the DW transition is gradually suppressed and superconductivity emerges, showing a domelike phase diagram with the maximum T_c of 3 K near $x \approx 0.04$.[7,8]

Since the SOC is proportional to Z^4, where Z is the atomic number, the superconductivity in doped $IrTe_2$ must associated with strong SOC due to the large Z. Therefore it is of great interest to investigate whether there is novel superconducting state in doped $IrTe_2$, as in $Cu_xBi_2Se_3$.[2,3] Furthermore, the phase diagram of doped $IrTe_2$ is reminiscent of high-T_c cuprates and some heavy fermion superconductors, in which superconductivity appears close to a magnetic quantum critical point (QCP). This means that there likely exists a QCP of charge-orbital DW under the superconducting dome of doped $IrTe_2$, and the DW fluctuations may give unconventional superconductivity.[9]

The ultra-low-temperature thermal conductivity measurement is a bulk tool to study the gap structure of superconductors.[10] The existence of a finite residual linear term κ_0/T in zero field is usually considered as the signature of nodal superconducting gap. Further information of nodal gap, gap anisotropy, or multiple gaps may be obtained from the field dependence of κ_0/T.[10] Previously, single-gap s-wave superconductivity near the QCP of charge DW has been clearly shown in Cu_xTiSe_2 by thermal conductivity measurements.[11]

In this Rapid Communication, we probe the superconducting gap structure of $Ir_{1-x}Pt_xTe_2$ by measuring the thermal conductivity κ of a single crystal down to 50 mK. Although a residual linear term κ_0/T is observed in zero field, the field dependence of κ_0/T shows unusual behavior different from a nodal superconductor. It decreases first in low field, then slowly increases in higher field. We attribute the finite κ_0/T in zero field and the decrease of κ_0/T in low field to the nonsuperconducting impure phase in the crystal, while the overall slow field dependence of κ_0/T is very similar to that in Cu_xTiSe_2, suggesting nodeless superconducting gap in $Ir_{1-x}Pt_xTe_2$.

Single crystals of $Ir_{1-x}Pt_xTe_2$ superconductors were grown by the flux method for the first time.[12] It is found that the homogeneous $Ir_{1-x}Pt_xTe_2$ single crystals with large superconducting volume fraction are very difficult to obtain, which is similar to the case of $Cu_xBi_2Se_3$.[1,13] Based on magnetic susceptibility measurements, the inhomogeneity of Pt content is apparent for different single crystals from the same batch and different parts from the same single crystal. Even for a small single crystal, different pieces cleaved along the c axis show different superconducting transition curves.

Despite of the inhomogeneity, we choose the best superconducting single crystal available, with the nominal composition $Ir_{0.8}Pt_{0.2}Te_2$. The sample was cleaved to a rectangular shape of dimensions 2.0 × 0.7 mm^2 in the

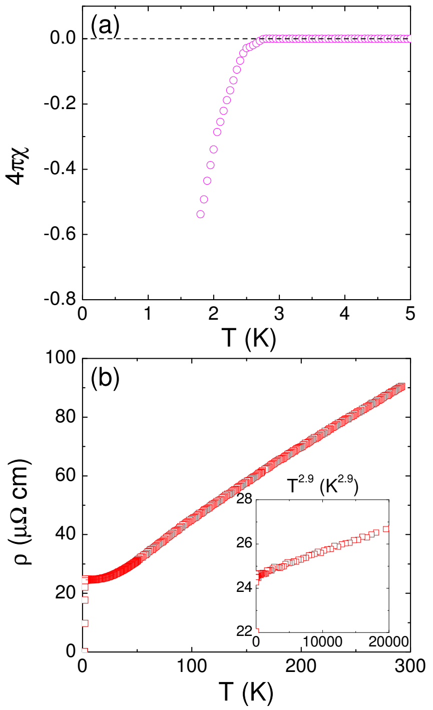

FIG. 1: (Color online). (a) The dc magnetic susceptibility of $Ir_{1-x}Pt_xTe_2$ single crystal with nominal $x = 0.20$. (b) In-plane resistivity of the nominal $Ir_{0.8}Pt_{0.2}Te_2$ single crystal. The data between 3 and 30 K can be fitted to $\rho(T) = \rho_0 + AT^n$, with $\rho_0 = 24.60 \pm 0.01$ $\mu\Omega$cm and $n = 2.9 \pm 0.1$. The inset is a plot of low temperature $\rho(T)$ vs $T^{2.9}$.

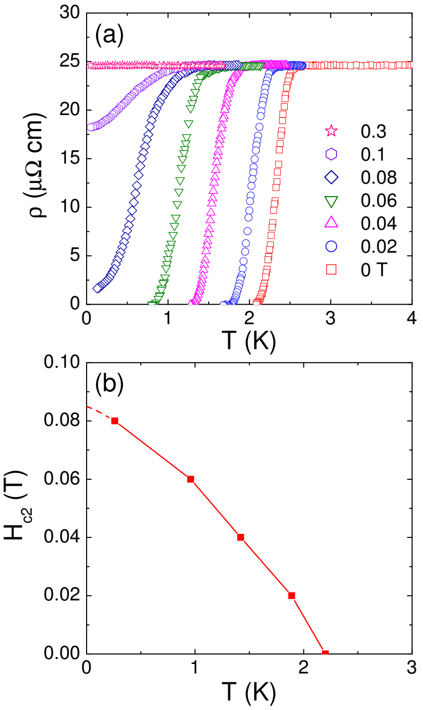

FIG. 2: (Color online). (a) Resistivity of the nominal $Ir_{0.8}Pt_{0.2}Te_2$ single crystal in magnetic field up to 0.3 T. (b) Temperature dependence of the upper critical field $H_{c2}(T)$, defined as the point dropping to 10% of the normal-state resistivity on the curves in (a). The dashed line is a guide to the eye, which points to $H_{c2}(0) \approx 0.085$ T.

ab plane, with 40 μm thickness along the *c* axis. The dc magnetic susceptibility was measured by using a SQUID (MPMS, Quantum Design). Four silver wires were attached to the sample with silver paint, which were used for both resistivity and thermal conductivity measurements. The contacts are metallic with typical resistance 10 mΩ at 2 K. In-plane thermal conductivity was measured in a dilution refrigerator, using a standard four-wire steady-state method with two RuO_2 chip thermometers, calibrated *in situ* against a reference RuO_2 thermometer. Magnetic fields were applied along the *c* axis and perpendicular to the heat current. To ensure a homogeneous field distribution in the sample, all fields were applied at temperature above T_c.

Figure 1(a) presents the dc magnetic susceptibility of $Ir_{1-x}Pt_xTe_2$ single crystal with nominal $x = 0.20$. It was measured in $H = 20$ Oe perpendicular to the *ab* plane, with zero field cooled. The onset of diamagnetic transition is at 2.7 K, and the transition does not complete down to 1.8 K. The superconducting volume fraction is about 55% at 1.8 K, showing bulk superconductivity of the sample. However, the wide transition indicates inhomogeneity of Pt content inside the sample.

Figure 1(b) shows the in-plane resistivity of the nominal $Ir_{0.8}Pt_{0.2}Te_2$ single crystal in zero field. The middle point of the resistive transition is at $T_c = 2.3$ K, in agreement with the susceptibility measurement. No resistivity anomaly is observed above T_c, which suggests that no DW transition occurs in our sample. Because the DW transition disappears near the optimal doping $x \approx 0.04$ in $Ir_{1-x}(Pd,Pt)_xTe_2$ system,[7,8] and the T_c of our sample is lower than the optimal $T_c \approx 3$ K, our sample should be on the overdoped side. Hereafter our sample is named OD20. The resistivity of OD20 between 3 and 30 K can be fitted to $\rho(T) = \rho_0 + AT^n$, with $\rho_0 = 24.60 \pm 0.01$ $\mu\Omega$cm and $n = 2.9 \pm 0.1$. The insert of Fig. 1(b) plots the low temperature $\rho(T)$ vs $T^{2.9}$, which is linear. Such a temperature dependence of $\rho(T)$ has been observed in $Ir_{1-x}Pt_xTe_2$ polycrystal and attributed to phonon-assisted interband scattering,[8] as in $TiSe_2$.[14]

Figure 2(a) shows the resistivity of OD20 in a magnetic field up to $H = 0.3$ T. The superconducting transition is gradually suppressed and no transition is observed down to 50 mK in $H = 0.3$ T. In Fig. 2(b), we plot the temperature dependence of the upper critical field H_{c2}, defined as the point dropping to 10% of the normal-state resistivity on the curves in Fig. 2(a). The dashed line is a guide to the eye, which points to $H_{c2}(0) \approx 0.085$ T. This value is half of the $H_{c2}(0) \approx 0.17$ T for optimally doped $Ir_{0.96}Pt_{0.04}Te_2$ polycrystal with $T_c = 3$ K.[8]

The in-plane thermal conductivity of OD20 in zero and finite magnetic fields are plotted in Fig. 3, as κ/T vs T. All the curves are roughly linear. Therefore we fit all the curves to $\kappa/T = a + bT^{\alpha-1}$ with α fixed to 2,

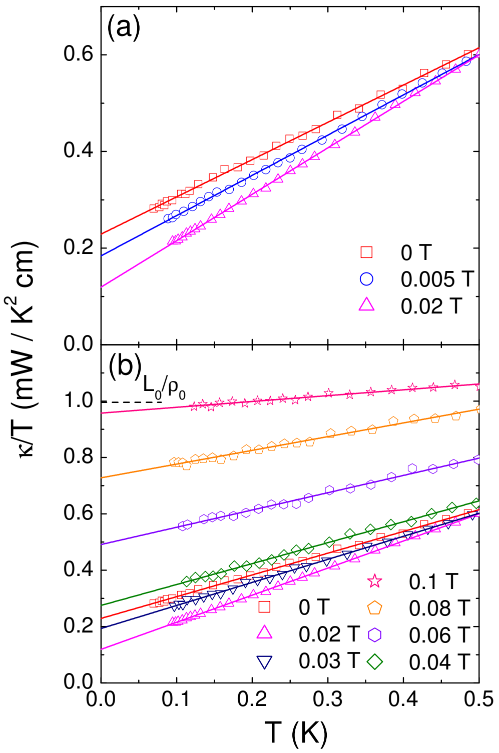

FIG. 3: (Color online). Low-temperature in-plane thermal conductivity of the nominal $Ir_{0.8}Pt_{0.2}Te_2$ single crystal in zero and magnetic fields applied along the c axis. The solid lines are fits to $\kappa/T = a + bT^{\alpha-1}$ with α fixed to 2. The dash lines are the normal-state Wiedemann-Franz law expectation L_0/ρ_0, with L_0 the Lorenz number 2.45 × 10^{-8} WΩK^{-2} and ρ_0 = 24.60 $\mu\Omega$cm, respectively.

in which the two terms aT and bT^{α} represent contributions from electrons and phonons, respectively.[15,16] The power α of the second term contributed by phonons is typically between 2 and 3, due to specular reflections of phonons at the boundary.[15,16] Previously $\alpha \approx 2.2$ was found in $Cu_{0.06}TiSe_2$,[11] and recently $\alpha \approx 2$ has been observed in some iron-based superconductors such as $BaFe_{1.9}Ni_{0.1}As_2$,[17] KFe_2As_2,[18] and $Ba(Fe_{1-x}Ru_x)_2As_2$ single crystals.[19] Here we only focus on the electronic term.

For OD20 in zero field, the fitting gives a residual linear term κ_0/T = 0.229 ± 0.001 mW K^{-2} cm^{-1}. This value is about 23% of the normal-state Wiedemann-Franz law expectation $\kappa_{N0}/T = L_0/\rho_0$ = 1.00 mW K^{-2} cm^{-1}, with L_0 the Lorenz number 2.45 × 10^{-8} WΩK^{-2} and normal-state ρ_0 = 24.60 $\mu\Omega$cm. Usually, a finite κ_0/T in zero field comes from nodal quasiparticles in a superconductor with nodal gap.[10] For example, κ_0/T = 1.41 mW K^{-2} cm^{-1} for the overdoped cuprate $Tl_2Ba_2CuO_{6+\delta}$ (Tl-2201), a d-wave superconductor with T_c = 15 K,[20] and κ_0/T = 17 mW K^{-2} cm^{-1} for the ruthenate Sr_2RuO_4, a p-wave superconductor with T_c = 1.5 K.[21] However, if some nonsuperconducting and metallic impure phase exists in a nodeless superconductor, it will also contribute a finite κ_0/T in zero field. For example, κ_0/T = 0.3 mW K^{-2} cm^{-1}, ∼7% of the normal-state value, was observed and attributed to the inclusions of pure graphite in the single-gap s-wave superconductor C_6Yb with T_c = 5.4 K.[22]

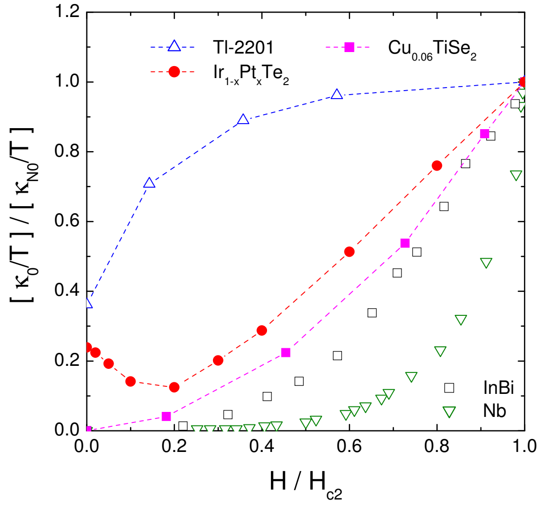

FIG. 4: (Color online). Normalized residual linear term κ_0/T of the nominal $Ir_{0.8}Pt_{0.2}Te_2$ single crystal as a function of H/H_{c2}. For comparison, similar data are shown for the clean s-wave superconductor Nb,[24] the dirty s-wave superconducting alloy InBi,[25] an overdoped d-wave cuprate superconductor Tl-2201,[20] and the single-gap s-wave superconductor $Cu_{0.06}TiSe_2$.[11]

Since we are aware that our single crystal is inhomogeneous, it is essential to check the field dependence of κ_0/T to distinguish between above two cases. In the case of nodal superconductor, κ_0/T increases rapidly ($\sim H^{1/2}$) in low field due to the Volovik effect,[23] as in Tl-2201.[20] However, in the case of single-gap s-wave superconductor containing nonsuperconducting impure phase, κ_0/T displays a slow field dependence, as in C_6Yb.[22] In Fig. 3, all the data of OD20 are fitted and κ_0/T is obtained for each magnetic field. Note that in the normal state of H = 0.1 T, the fit gives κ_0/T = 0.96 ± 0.01 mW K^{-2} cm^{-1}, which roughly satisfies the Wiedemann-Franz law. The bulk $H_{c2}(0)$ is determined as 0.1 T, slightly higher than $H_{c2}(0)$ = 0.085 T from the resistivity data in Fig. 2. A slightly different $H_{c2}(0)$ does not affect our discussion on the field dependence of κ_0/T below.

In Fig. 4, the normalized κ_0/T of OD20 is plotted as a function of H/H_{c2}. For comparison, we also plot the data of the clean s-wave superconductor Nb,[24] the dirty s-wave superconducting alloy InBi,[25] the d-wave cuprate superconductor Tl-2201,[20] and the s-wave superconductor $Cu_{0.06}TiSe_2$.[11] From Fig. 4, κ_0/T of OD20 deceases at low field first, then it increases slowly above $H \approx 0.02$ T. Such a behaviour of κ_0/T is distinctly different from nodal superconductor Tl-2201. In fact, the slow field dependence above 0.02 T is rather very similar to that of single-gap s-wave superconductor $Cu_{0.06}TiSe_2$. Therefore, we attribute the finite κ_0/T of OD20 in zero field to nonsuperconducting impure phase, and the overall slow field dependence of κ_0/T manifests the underlying nodeless superconducting gap, as in C_6Yb.[22]

Since our sample is on the overdoped side ($x > 0.04$), and the $Ir_{1-x}Pt_xTe_2$ is nonsuperconducting for $x > 0.10$, the nonsuperconducting impure phase in our sample should have the doping level higher than 0.10. By assuming the same ρ_0 for different doping level in our sample, some 23% volume fraction of nonsuperconducting impure phase will give the κ_0/T in zero field that is 23% of the normal state. Since the magnetoresistance of our sample is negligible, the decrease of κ_0/T in low field should not come from the magnetoresistance effect of the nonsuperconducting impure phase. Actually, it may be explained by vortex scattering. Above the lower critical field H_{c1}, the vortex will enter into the sample, which will scatter those normal electrons contributed by the nonsuperconducting impure phase, and reduce the κ_0/T. According to our data, the H_{c1} could be as low as 0.002 T. This is possible, since some part of our sample may have very low T_c due to the inhomogeneity.

Nodeless gap does not essentially mean conventional superconductivity. For example, the nodeless gap observed in optimally doped iron-based superconductor may be unconventional $s_{\pm}$-wave resulting from antiferromagnetic spin fluctuations.[26] However, here in $Ir_{1-x}Pt_xTe_2$, the nodeless gap is unlikely $s_{\pm}$-wave, despite that there may exist charge-orbital DW fluctuations.[7] One obvious reason is that $Ir_{1-x}Pt_xTe_2$ does not have that kind of multiple Fermi surfaces as iron-based superconductors.[7,26] Since previously nodeless superconductivity has been observed in Cu_xTiSe_2 associated with a QCP of charge DW, it may not come as a surprise that we observe nodeless superconductivity again in $Ir_{1-x}Pt_xTe_2$ with a QCP of charge-orbital DW. In both systems, the appearence of superconductivity may have little to do with the DW fluctuations.

From the aspect of strong SOC, an unconventional odd-parity pairing state was claimed for the promising topological superconductors $Cu_xBi_2Se_3$.[2,3] However, both nodeless gap or gap with point nodes are allowed for the odd-parity superconducting state.[2] In this context, our finding of nodeless superconductivity in $Ir_{1-x}Pt_xTe_2$ with strong SOC does not completely exclude novel superconducting state. More experiments are needed to clary this issue.

In summary, we investigate the superconducting gap structure of overdoped superconducting $Ir_{1-x}Pt_xTe_2$ single crystal by thermal conductivity measurements. The overall slow field dependence of κ_0/T supports nodeless superconductivity, while the finite κ_0/T in zero field and the decrease of κ_0/T in low field are attributed to the nonsuperconducting impure phase in the crystal. Our result puts a strict constrain on the paring symmetry of this system, when one considers the effect of strong spin-orbital coupling and density-wave fluctuations on superconductivity.

This work is supported by the Natural Science Foundation of China, the Ministry of Science and Technology of China (National Basic Research Program No: 2009CB929203 and 2012CB821402), and the Program for Professor of Special Appointment (Eastern Scholar) at Shanghai Institutions of Higher Learning. The research at Postech and Rutgers University was supported by the Max Planck POSTECH/KOREA Research Initiative Program [Grant No. 2011-0031558] through NRF of Korea funded by MEST and the NSF under Grant No. NSFDMR-1104484, respectively.

* E-mail: shiyan_li@fudan.edu.cn

---

[1] Y. S. Hor, A. J. Williams, J. G. Checkelsky, P. Roushan, J. Seo, Q. Xu, H.W. Zandbergen, A. Yazdani, N. P. Ong, and R. J. Cava, Phys. Rev. Lett. **104**, 057001 (2010).

[2] S. Sasaki, M. Kriener, K. Segawa, K. Yada, Y. Tanaka, M. Sato, and Y. Ando, Phys. Rev. Lett. **107**, 217001 (2011).

[3] M. Kriener, Kouji Segawa, Satoshi Sasaki, and Yoichi Ando, arXiv:1206.6260.

[4] P. Badica, T. Kondo, and K. Togano, J. Phys. Soc. Jpn. **74**, 1014 (2005).

[5] H. Q. Yuan, D. F. Agterberg, N. Hayashi, P. Badica, D. Vandervelde, K. Togano, M. Sigrist, and M. B. Salamon, Phys. Rev. Lett. **97**, 017006 (2006).

[6] M. Nishiyama, Y. Inada, and Guo-qing Zheng, Phys. Rev. Lett. **98**, 047002 (2007).

[7] J. J. Yang, Y. J. Choi, Y. S. Oh, A. Hogan, Y. Horibe, K. Kim, B. I. Min, and S-W. Cheong, Phys. Rev. Lett. **108**, 116402 (2012).

[8] S. Pyon, K. Kudo, and M. Nohara, J. Phys. Soc. Jpn. **81**, 053701 (2012).

[9] P. Monthoux and G. G. Lonzarich, Phys. Rev. B **69**, 064517 (2004).

[10] H. Shakeripour, C. Petrovic and L. Taillefer, New J. Phys. **11**, 055065 (2009).

[11] S. Y. Li, G. Wu, X. H. Chen, and Louis Taillefer, Phys. Rev. Lett. **99**, 107001 (2007).

[12] J. J. Yang, Y. S. Oh, and S-W. Cheong, unpublished.

[13] M. Kriener, K. Segawa, Z. Ren, S. Sasaki, S. Wada, S. Kuwabata, and Y. Ando, Phys. Rev. B **84**, 054513 (2011).

[14] A. F. Kusmartseva, B. Sipos, H. Berger, L. Forró, and E. Tutiš, Phys. Rev. Lett. **103** 236401 (2009).

[15] M. Sutherland, D. G. Hawthorn, R. W. Hill, F. Ronning, S. Wakimoto, H. Zhang, C. Proust, E. Boaknin, C. Lupien, Louis Taillefer, Ruixing Liang, D. A. Bonn, W. N. Hardy, Robert Gagnon, N. E. Hussey, T. Kimura, M. Nohara, and H. Takagi, Phys. Rev. B **67**, 174520 (2003).

[16] S. Y. Li, J.-B. Bonnemaison, A. Payeur, P. Fournier, C. H. Wang, X. H. Chen, and L. Taillefer, Phys. Rev. B **77**, 134501 (2008).

[17] L. Ding, J. K. Dong, S. Y. Zhou, T. Y. Guan, X. Qiu, C. Zhang, L. J. Li, X. Lin, G. H. Cao, Z. A. Xu and S. Y. Li, New J. Phys. **11**, 093018 (2009).

[18] J. K. Dong, S. Y. Zhou, T. Y. Guan, H. Zhang, Y. F. Dai,

X. Qiu, X. F. Wang, Y. He, X. H. Chen, and S. Y. Li, Phys. Rev. Lett. **104**, 087005 (2010).

[19] X. Qiu, S. Y. Zhou, H. Zhang, B. Y. Pan, X. C. Hong, Y. F. Dai, Man Jin Eom, Jun Sung Kim, Z. R. Ye, Y. Zhang, D. L. Feng, and S. Y. Li, Phys. Rev. X **2**, 011010 (2012).

[20] C. Proust, E. Boaknin, R. W. Hill, Louis Taillefer, and A. P. Mackenzie, Phys. Rev. Lett. **89**, 147003 (2002).

[21] M. Suzuki, M. A. Tanatar, N. Kikugawa, Z. Q. Mao, Y. Maeno, and T. Ishiguro, Phys. Rev. Lett. **88**, 227004 (2002).

[22] M. Sutherland, N. Doiron-Leyraud, Louis Taillefer, T. Weller, M. Ellerby, and S. S. Saxena, Phys. Rev. Lett. **98**, 067003 (2007).

[23] G. E. Volovik, JETP Lett. **58**, 469 (1993).

[24] J. Lowell and J. Sousa, J. Low. Temp. Phys. **3**, 65 (1970).

[25] J. Willis and D. Ginsberg, Phys. Rev. B **14**, 1916 (1976).

[26] P. J. Hirschfeld, M. M. Korshunov, and I. I. Mazin, Rep. Prog. Phys. **74**, 124508 (2011).